Published in final edited form as:
Acta Biomater. 2012 May ; 8(5): 1693–1702. doi:10.1016/j.actbio.2012.01.012.

Gel Microstructure Regulates Proliferation and Differentiation of MC3T3-E1 Cells Encapsulated in Alginate Beads

Baek-Hee Lee[1,2], **Bing Li**[1,2,§], and **Scott A. Guelcher**[1,2,3,*]

[1]Department of Chemical and Biomolecular Engineering, Vanderbilt University, Nashville, TN

[2]Center for Bone Biology, Vanderbilt University Medical Center, Nashville, TN

[3]Department of Biomedical Engineering, Vanderbilt University, Nashville, TN

Abstract

For cell transplantation into damaged tissues, viable cells must be delivered to the defect site in a suitable carrier. However, the hypoxic and nutrient-limited environment in the carrier can induce massive cell death. The aims of this study were to increase the viability and regulate the behavior of osteoprogenitor cells encapsulated in alginate hydrogels through control of the gel microstructure. Cell survivability in alginate beads was improved through the use of α-MEM as the solvent for alginic acid sodium salt and $CaCl_2$ solutions, which supplied additional nutrients for the cells compared to water or buffer. The mesh size and shear modulus of the hydrogel were hypothesized to regulate proliferation and differentiation of osteoprogenitor cells. MC3T3-E1 cells demonstrated enhanced osteoblast differentiation when encapsulated in high-density alginate with smaller mesh size and more rigid mechanical properties, as confirmed by increased alkaline phosphatase activity and osteocalcin secretion. However, MC3T3-E1 cells encapsulated in low-density alginate beads with a larger mesh size and more compliant mechanical properties exhibited increased proliferation. These results demonstrate that the microstructure of alginate hydrogels can regulate the behavior of osteoprogenitor cells, thus suggesting that the tuning the properties of the gel may be a useful approach for enhancing new bone formation.

Keywords

alginate; encapsulation; microstructure; differentiation; proliferation; MC3T3-E1 cells

1. Introduction

Various therapeutic delivery systems have been investigated as treatments for diseases and tissue regeneration [1–9]. Recently, there has been extensive research in the transplantation of living cells into damaged tissues for tissue repair [4–7]. Cell delivery approaches currently under investigation include both direct injection of cells and also delivery of cells within an implanted scaffold [4–7]. However, cells injected directly into the tissue defect can migrate away from the wound and implantation of scaffolds seeded with cells requires

*Corresponding author: PMB 351604, 2301 Vanderbilt Place, VU Station B #351604, Nashville, TN 3723, USA. Tel.: +1-615-322-9097; fax: +1-615-343-7951. scott.guelcher@vanderbilt.edu.
§Currently at GE Global Research Center, One Research Circle, CEB 1545, Niskayuna NY, 12309

invasive surgical techniques [6–9]. In addition, massive cell death induced by the hypoxic and nutrient-limited environment, as well as poor incorporation and integration of the delivered cells, are significant limitations of conventional cell delivery systems [2, 7].

Cell encapsulation in alginate hydrogels represents one of the most widely investigated approaches for cell therapy [10, 11]. Alginate consists of a 3D polymeric network with high water content, which imparts structural and mechanical similarities to macromolecular-based components in natural tissues [11]. The 3D structure of alginate not only facilitates the diffusion of body fluids including nutrients, oxygen and metabolites, but also protects the encapsulated cells against shear forces, chemical reactions, and attack by inflammatory cells [10–14].

Cell-cell contact generally arrests cell growth through contact inhibition [14–17]. For example, relatively large islands of 2D substrates coated with the extracellular matrix (ECM) protein laminin promoted proliferation, while relatively small islands induced apoptosis [15, 17]. Similarly, cell-substrate and cell-cell interactions within 3D gel networks have been suggested to play a critical role in regulating cell proliferation, differentiation, and organ size [18–20]. Encapsulation of cells in alginate beads has been investigated extensively due in part to the flexibility of the process, where in the physicochemical properties of the gels such as biodegradability, bead size, swelling, gel mesh size, mechanical properties, and cell seeding density can be controlled by varying the chemical composition and processing parameters [11, 21–24].

To promote cell adhesion, proliferation, and differentiation, alginate is frequently modified with cell adhesion peptides and proteins [1, 25–28]. Specifically, the peptidearginine–glycine–aspartic acid (RGD), which is derived from the extracellular matrix (ECM) protein fibronectin, has been coupled to alginate gels at tunable densities to control cell adhesion and differentiation [29–31]. The microstructure of the alginate gel is also anticipated to regulate cellular behavior, considering that the hydrated 3D network allows cells to adhere, spread, migrate, and interact with other cells [11, 32]. Varying the encapsulation conditions has been suggested to provide control over both the diffusion of molecules into the alginate matrix, as well as control over the porosity of the matrix to permit the proliferation and growth of encapsulated mouse embryonic stem cells within the alginate beads [11].

In the present study, the effects of the physical microenvironment, including the mesh size and shear modulus of the gel, on cellular proliferation and differentiation were investigated in alginate gels without modification by peptides. The crosslink density of the gels, which controls the mesh size and shear modulus, was adjusted by varying the concentrations of the alginic acid and calcium chloride solutions. Considering previous studies reporting that the elastic modulus of the matrix affects cellular outcomes in both 2D and 3D culture [33–36], we hypothesized that the mesh size and shear modulus of the gel regulate proliferation and differentiation of cells encapsulated in the alginate beads [37, 38]. To increase cell viability during the encapsulation process, α-minimum essential medium (α-MEM) was incorporated in alginate beads, which was anticipated to enhance the availability of nutrients for encapsulated cells during the synthesis process. Viability, proliferation, and osteogenic differentiation of MC3T3-E1 preosteoblast cells were measured *in vitro* to determine how the microstructure of the alginate gels regulates cell fate in 3D cell culture.

2. Materials and Methods

2.1. Alginate beads for cell encapsulation

Alginic acid sodium salt (viscosity 20,000~40,000 cP, molecular weight 120 – 190 kDa, Aldrich, St. Louis, MO) was dissolved in DI-water and in α-MEM at concentrations of 1 and

2% (w/v). Briefly, MC3T3-E1 cells (1×10^6 cells/ml) were suspended in the alginic acid sodium salt solutions (1 and 2% (w/v)) and mixed for 2 h. Cell viability was measured by live/dead staining before and after incubation in alginic acid solution and found to be unchanged. Suspensions of cells in alginate were then added drop-wise into two different crosslinker solutions: (a) $CaCl_2$ in DI-water or (b) $CaCl_2$ in α-minimum essential medium (MEM) at room temperature. The concentration of $CaCl_2$ solutions was either 100 or 200 mM. The beads formed in the microencapsulation device were subsequently cured in the $CaCl_2$ solution for 1 h. Each formulation of alginate beads was designated as *A*–*B*, where *A* represents the concentration of the alginate solution (1 or 2 wt%) and *B* denotes the concentration of $CaCl_2$ solution (100 or 200 mM). For example, composition 1-100 corresponds to alginate beads synthesized with 1 wt% alginate solution and 100 mM $CaCl_2$ solution.

2.2. Swelling experiments and calculation of mesh size of alginate beads

Four alginate bead compositions were investigated as summarized in Table 1. The alginate solution was added drop-wise into the $CaCl_2$ solution in DI-water (100 or 200 mM). Images of 30 beads obtained by optical microscopy (OM) were analyzed using an Olympus DP71 camera attached to a fluorescent microscope (Olympus CKX41, U-RFLT50, Center Valley, PA) to measure bead size and analyze cell morphology. The beads were incubated in DI-water at 37°C and bead size measured as a function of time for up to 10 days. The swelling ratio and mesh size of each alginate bead composition were calculated from swelling experiments as previously described [39–43]. Five beads were incubated in DI-water at 37°C, dried under vacuum, and weighed. The swelling ratio q_F and volume fraction polymer ν_2 were calculated from Eqs. (1) and (2) [44]:

$$q_F = \frac{\text{mass of gel after preparation (wet)}}{\text{mass of gel after drying (dry)}} \tag{1}$$

$$\nu_2 = 1 + (q_F - 1)\rho_P/\rho_W \tag{2}$$

where ρ_P is the density of the alginate polymer (1.601 g/cm^3) and ρ_W is the density of water (1.0 g/cm^3).

The crosslink density n was calculated from the Flory-Rehner equation (Eq. (3)) [39, 40]:

$$n = -[\ln(1-\nu_2) + \nu_2 + \chi_1\nu_2^2]/[V_1(\nu_2^{1/3} - 0.5\nu_2)] \tag{3}$$

where χ_1 is the Flory-Huggins interaction parameter (~0.5), V_1 is the molar volume of the solvent (water, 18 cm^3), and n represents the number of active network chain segments per unit volume (mol cm^{-3}) [43, 45]. The molecular weight between crosslinks is then given by Eq. (4):

$$M_c = \rho_P/n \tag{4}$$

Due to the high density of the alginate network, permeability experiments for measuring the pore size in the gel were not feasible [41]. The corresponding mesh size, ξ, can be subsequently approximated using Eq. (5) [39–43]:

$$\xi = \nu_2^{-1/3} l^* (2M_c/M_r)^{1/2} C_n^{1/2} \tag{5}$$

where M_r is the molecular weight (390.1 g/mol) of the repeat unit, *l* is the carbon-carbon bond length of monomer unit (assumed to be 5.15 Å), and C_n is the characteristic ratio for alginate calculated as $Cn = 0.021*M_n + 17.95 = 21.1$ [43, 45]. The mesh size effectively represents the maximum diameter of a molecule that can diffuse through the ideal network.

2.3. Cell culture for the encapsulated cells in alginate beads

Cells encapsulated in alginate beads were cultured in either standard culture medium or osteogenic culture medium, which consisted of α-MEM, 2.5% (v/v) FBS, 1% (v/v) penicillin (100 U/ml)/streptomycin (100 μg/ml), 50 μg/ml L-ascorbic acid, and 10 mM β-glycerophosphate, in the incubator with 5% CO_2 at 37°C. Cell culture was performed under dynamic conditions using an orbital shaker operated at 100 rpm at 37°C. Sample analysis or preparation for qualitative assessment performed on days 1, 2, 5, 10, and 15. The medium was replaced every 2 days, and the cells were recovered from the beads as described in Section 2.7.

2.4. Rheological measurements

The storage and loss moduli of alginate gels were measured under shear conditions at 25°C using a TA Instruments AR-G2 Rheometer (TA Instruments, New Castle, DE) fitted with parallel plates (diameter of 25 mm, gap of 1 mm) [46]. Disk-shaped alginate gels were prepared by adding 1 ml alginic acid sodium salt solution (1 or 2% (w/v) in DI-water) to a mixing cup and reacted with 10 ml of $CaCl_2$ crosslinker solution in DI-water (100 or 200 μM). The alginate gels were fully reacted for 12 h at room temperature. Shear storage and loss moduli were measured by oscillatory shear experiments performed with strain amplitude of 1.5% and oscillation frequency of 10 rad/s, which is within the linear viscoelasticity region as verified by frequency and strain sweeps following each measurement. The molecular weight between crosslinks was calculated from the measured value of the shear modulus (G) using the following equation [24, 47]:

$$M_{c,R} = \frac{c_P RT}{G} \tag{6}$$

where c_P is the concentration of alginate in solution (1 or 2 wt%), R is the gas constant (8.314 m^3 Pa mol^{-1} K^{-1}), and T is the temperature.

2.5. Cell viability

4 mM cell-permeable calcein acetoxymethyl (Calcein AM) and 2 mM ethidium homodimer-1 (EthD-1) from the Live/Dead Viability/Cytotoxicity Kit (Invitrogen) for mammalian cells was added to the samples. Calcein AM produces a bright green fluorescence in live cells. Ethidium homodimer-1 is retained within damaged or dead cells, imparting a bright red fluorescence. Fluorescence images were observed by an Olympus DP71 camera attached to a fluorescent microscope (Olympus CKX41, U-RFLT50, Center Valley, PA). Cell viability (the percentage of viable cells) was measured by counting the numbers of live and dead cells from the fluorescent images at time points of 0, 1, 2, 5, and 10 days.

2.7. Alkaline phosphatase activity and total protein

Five alginate beads were harvested from 24-well plates at days 1, 2, 5, 10, and 15 and immersed in phosphate-buffered saline (PBS) for 5 min followed by washing with PBS three times. The washed beads were crushed and lysed with 150 μl of 0.05% Triton X-100. The plates were homogenized by three freeze-thaw cycles. After removing the lysate, the alginate fragments were viewed in the microscope and no evidence of cells was apparent.

The lysates (20 μl) were added to 96-well plates with 100 μl substrate buffer (2 mg/ml disodium p-nitrophenylphosphate hexahydrate and 0.75 M 2-amino-2-methyl-1-propanol). The mixtures were then incubated for 30 min at 37°C and the resulting optical absorbance measured at 410 nm by using a mQuant spectrophotometer (Bio-Tek Instruments Inc.). ALP activity was determined from a standard curve generated by employing the reaction of a p-nitrophenyl solution. The ALP activity was normalized using the measured total protein to account for differences in the number of cells on different alginate beads at individual time points. Total cellular protein was determined with a BCA protein assay kit (Pierce). The lysates (10 μl) were mixed with 200 μl BCA working reagent containing cupric sulfate and bicinchoninic acid in 96-well plates, and then incubated for 30 min at 37°C. The resulting optical absorbance was measured at 562 nm with the μQuant spectrophotometer. Total protein amounts were calculated with a standard curve, which was generated with bovine serum albumin.

2.8. Osteocalcin release

Osteocalcin (OCN) secretion from encapsulated MC3T3-E1 cells in alginate beads was measured as a later marker of osteogenic differentiation. Secreted OCN was measured from the standard and osteogenic culture media at 16 days by an enzyme immuno assay (mouse osteocalcin EIA kit BT 470, Biomedical Technologies, Inc.) using the instructions in the kit. The absorbance was measured at 450 nm with the μQuant spectrophotometer. Mouse OCN was used to generate a standard curve, which was prepared from 7 OCN standards. The concentration of OCN was determined by interpolation and normalized by total protein.

2.9 Proliferation and differentiation rates

The rates of proliferation and differentiation were calculated from the total protein (TP, mg/ml) and alkaline phosphatase activity normalized by total protein (ALP/TP, U/(mg*ml)) versus time data:

$$\begin{aligned} r_P &= \frac{d}{dt}(TP) \\ r_D &= \frac{d}{dt}(ALP/TP) \end{aligned} \tag{7}$$

Both TP and ALP/TP data were assumed to be linear functions of time, and thus the values of r_P and r_D were calculated from the slopes of the TP and ALP/TP versus time plots, respectively. The ratio of the dimensionless proliferation rate to the dimensionless differentiation rate was calculated as follows:

$$r_{P/D} = \frac{r_P'}{r_D'} = \frac{r_P/TP_1}{r_D/(ALP/TP)_1} \tag{8}$$

where TP_1 and $(ALP/TP)_1$ denote the TP and ALP/TP values measured on day 1.

2.10. Statistical Analysis

All data are presented as mean standard deviation (±S.D.). One way ANOVA with bonferroni correction ($p < 0.05$) was used for evaluation of statistical significance for all data.

3. Results

3.1. Effects of medium on cell viability

Encapsulation of MC3T3-E1 cells in 3D alginate beads was performed with two kinds of solvents, DI water and α-MEM, for the alginate and $CaCl_2$ solutions. The viability of cells encapsulated in beads prepared with α-MEM solvents during the synthesis process exceeded 98%, while in the beads synthesized with DI water solutions the viability was <65%. When synthesized in the presence of DI water, cells are exposed to a nutrient-limited environment for at least 4 h, which is conjectured to result in increased cell death compared to synthesis in the presence of α-MEM.

3.2. Effects of alginate composition on swelling, gel mesh size, and mechanical properties

Gels with a larger mesh size and lower shear modulus were anticipated to facilitate proliferation, while gels with a smaller mesh size were expected to spatially constrain the cells and promote differentiation. The initial sizes of the 1-100, 1-200, 2-100 and 2-200 alginate beads measured by image analysis were 2.072 ± 0.026, 2.085 ± 0.028, 2.263 ± 0.029 and 2.201 ± 0.028 mm, respectively. As shown in Figure 1A, the diameter of all four compositions of alginate beads increased from day 1 to day 10. Figure 1B displays the mass swelling ratio as a function of the immersion time in DI water for all four alginate compositions. Consistent with the increase in bead size with time, the swelling ratio increased with time for all four compositions. The swelling ratio is related to the crosslink density by the Flory-Rehner equation, which predicts that swelling increases with the molecular weight between crosslinks. While mammals lack the enzyme alginase that cleaves alginate chains, ionically cross-linked alginate gels dissolve by release of the divalent Ca^{2+} ions into the surrounding media resulting from cation exchange with monovalent sodium ions [48]. Thus, when the beads are immersed in DI water, the Ca^{2+} crosslinks break down, resulting in an increase in the molecular weight between crosslinks. The initial mesh sizes (ξ) of the 1-100, 1-200, 2-100 and 2-200 alginate beads were 19.8 ± 2.8, 16.3 ± 0.3, 9.4 ± 0.6 and 4.3 ± 0.4 nm, respectively. As expected, the calculated gel mesh size (Figure 1C) decreased with increasing concentration of both alginate and calcium solutions, and increased with time when incubated in DI water for 10 days (Figure 1C). For example, the mesh size of 1-100 beads increased from 19.8 ± 2.8 nm to 240.2 ± 18.9 nm after 10 days of incubation in DI-water. In contrast, the mesh size of 2-200 beads showed a substantially smaller increase in mesh size (4.3 to 33.8 nm) compared to the 1-100 beads.

The alginate composition also controlled the initial mechanical properties of the gels, as evidenced by the increase in shear modulus with increasing calcium and alginate concentration (Figure 2). For example, formulation 1-100 had the lowest elastic modulus (3.91 kPa), while formulation 2-200 had the highest elastic modulus (18.4 kPa). As shown by Eq (6), the shear modulus scales with M_c^{-1} and $\xi^{-1/2}$. The initial values of ξ calculated from the initial shear modulus data are ~50% greater than those calculated from the swelling data (Table 1). Thus the microstructure and mechanical properties of the gels are inter-related and can be controlled by changing the concentrations of the alginate and $CaCl_2$ solutions.

3.3. Effect of alginate composition on cell proliferation

To investigate the effects of gel microstructure on cell fate, we performed optical microscopy (OM) with fluorescent staining. Representative OM and live/dead (L/D) staining images of 1-100 alginate beads show that low-density alginate beads characterized by a larger mesh size supported proliferation of the encapsulated MC3T3-E1 cells (Figure 3, 1-100 alginate beads). Mitosis began after day 1, and small clusters of cells were observed after day 4 (Figure 3, 1-100 alginate beads). At 16 days, large clusters of MC3T3-E1 cells

formed as a result of proliferation (Figure 3, 1-100 alginate beads). There was no evidence of apoptotic features such as cell shrinkage or dead cells (red fluorescence) in the clusters. In contrast, the high-density 2-200 beads did not reveal evidence of clustering at day 1, 4, or 10 (Figure 3, 2-200 alginate beads).

Figure 4 presents total protein measured in 5 alginate beads cultured under dynamic conditions as a function of immersion time in the standard and osteogenic culture media. Total protein in the low-density alginate beads (1-100 and 1-200) increased significantly over the culture period. Furthermore, at each time point there was significantly more total protein in the less crosslinked, compliant 1-100 alginate beads than in the 2-200 alginate beads ($P<0.05$). In contrast, total protein measured for the high-density alginate beads (2-100 and 2-200) with small mesh size did not increase significantly up to 15 days (Figure 4, 2 wt% row). Thus proliferation of the encapsulated cells was greatest in the alginate beads with the lowest density, highest shear modulus, and largest large mesh size.

3.4. Effect of alginate composition on cell differentiation

Alkaline phosphatase (ALP) activity and osteocalcin (OCN) assays were used to evaluate osteogenic differentiation of the encapsulated MC3T3-E1 cells in the four types of alginate beads (Figures 5 – 6). ALP and OCN are early- and late-stage markers of osteoblast differentiation, respectively [32]. By day 15, the 1-100 and 1-200 beads had degraded and fractured under dynamic cell culture conditions using the standard culture medium, resulting in release of cells which subsequently attached to the well plate. Thus it was not possible to measure total protein and ALP activity after 15 days for the 1-100 and 1-200 beads. As shown in Figure 5, in standard culture medium ALP activity (normalized by total protein, TP) was relatively constant with time at ~0.1 U/mg/min in 1-100 and 1-200 beads, while in 2-100 and 2-200 beads it increased with time up to >0.4 U/mg/min. Similarly, OCN expression in the 2-200 beads with the smallest initial mesh size (4.3 nm) was significantly higher than that in all other beads as shown in Figure 6A ($P<0.05$). In osteogenic medium, ALP/TP increased with time for all groups, and activity was higher in the 2-100 and 2-200 beads. Similarly, OCN expression was significantly higher for each treatment group when cultured in osteogenic medium compared to standard medium, and was significantly higher in 2-100 and 2-200 beads compared to the 1 wt% alginate beads (Figure 6B). Taken together, the data in Figures 5 and 6 suggest that differentiation was dominant in rigid low-density beads with small mesh size, while proliferation was dominant in compliant low-density beads with larger mesh size when cells were cultured in α-MEM.

3.5 Effects of the gel microstructure on the rates of cell proliferation and differentiation

Total protein (TP, mg/ml) and ALP/TP (U/mg/min) are plotted versus the initial mesh size in Figure 7. In standard medium, TP increases with mesh size for the 1-100 and 1-200 gels, while it is relatively constant for the 2-100 and 2-200 gels. In contrast, ALP/TP increases with initial mesh size for the 2-100 and 2-200 gels, while it is relatively constant for the 1-100 and 1-200 gels. In osteogenic medium, TP is relatively constant with mesh size and ALP/TP increases with mesh size. However, the increase in mesh size ξ with time due to dissolution of the gel confounds the interpretation of the proliferation and differentiation data shown in Figure 7. To more clearly show the effects of initial mesh size on cell fate, the rates of proliferation and differentiation calculated from Eq (7) are plotted versus initial mesh size in Figure 8. The proliferation rate r_P increases dramatically with initial mesh size, while the differentiation rate r_D decreases strongly with increasing initial mesh size in standard medium. These observations support the notion that the relatively large (e.g., >16 nm) initial mesh size of the 1-100 and 1-200 gels supports cell proliferation, while the smaller (e.g., <10 nm) initial mesh size of the 2-100 and 2-200 gels supports cell differentiation. In osteogenic medium, the differentiation rate decreases with initial mesh

size, which suggests that the mesh size regulates differentiation even in the presence of osteogenic medium.

4. Discussion

In this study, MC3T3-E1 osteoprogenitor cells were encapsulated in alginate beads with varying mesh size and shear modulus to investigate the effects of the microstructure of the gel on cell proliferation and differentiation. By varying the concentration of the alginate and $CaCl_2$ precursor solutions, gels with initial mesh sizes ranging from 4 – 20 nm were synthesized. After 10 days of incubation time in α-MEM, the mesh size increased for all four alginate compositions, ranging from 30 to 250 nm. Cellular proliferation (calculated from measurements of total protein versus time) was greatest in the compliant 1-100 and 1-200 beads with mesh size > 16 nm, while cellular differentiation (calculated from measurements of ALP/TP versus time) was greatest in the rigid 2-100 and 2-200 beads with mesh size < 9 nm. Encapsulation of the MC3T3-E1 cells using alginate and $CaCl_2$ solutions prepared from α-MEM increased the initial cell viability to >98% from the value of 60% observed when the precursor solutions were prepared from DI water. The increase in cell viability was attributed to the availability of nutrients provided by α-MEM during the entire encapsulation process.

The initial mesh sizes calculated from the Flory-Rehner equation decreased with increasing concentration of alginic acid and $CaCl_2$. The Flory-Rehner equation is derived from rubber elasticity theory, which assumes that the polymer network comprises Gaussian chains connected by point crosslinks [43]. However, the crosslinks in alginate are elongated junction zones, not points. Furthermore, the Flory-Rehner equation does not account for other non-idealities, such as a non-affine network, solvent-polymer volume exclusion effects, and non-ideal Donnan ionic effects [43, 46]. Thus, the mesh size calculated from Eqs (5) and (6) is an approximation of the actual pore size in an alginate gel [41]. While the mesh size decreased with M_c, the shear modulus G of the gels increased with decreasing M_c. For the 1-200 gel, G = 5.9 kPa and M_c = 4241 g/mol, which is in reasonable agreement with a previous study reporting 1% methacrylated alginate gels (7.6% methacrylation) having shear modulus 11.4 kPa and M_c = 4335 g/mol [24]. The values of ξ calculated from the rheology data were ~1.5 times greater than those calculated from the Flory-Rehner equation. Thus the rheology experiments generally predicted a larger molecular weight between cross-links and network mesh size than the swelling experiments. The limited applicability of the Flory-Rehner theory to alginate gels may contribute to the discrepancy in initial mesh sizes measured by the swelling and rheology experiments.

Considering that the cells (~10 – 20 μm) are 3 orders of magnitude larger than the initial mesh size (3 – 20 nm) of the network, cross-linking of the alginate around the cells is anticipated to result in micron-size defects in which the cells are embedded. When incubated in buffer or water (e.g., Ca^{2+}-free medium), diffusion of the divalent ions (e.g., Ca^{2+}) ionically cross-linking the gel into the surrounding medium can result in dissolution of the gel, which is consistent with the data in Figure 1A and B showing an increase in bead size and swelling when incubated in α-MEM for up to 10 days. Swelling of alginate gels can be associated with changes in chain stretching and conformation [49, 50], which contribute to the increase in mesh size with swelling [51] predicted by the Flory-Rehner equation as shown in Figure 1C. Thus as the crosslinks degrade, the micron-size defects resulting from the presence of the cells are conjectured to grow in size, thereby creating additional space in which cells can proliferate. This notion is consistent with the observed increase in cell proliferation with increasing rate of crosslink degradation (approximated by $d\xi/dt$) in Figure 9A.

To further investigate how the properties of the alginate gels regulate cell fate, the dimensionless ratio of proliferation to differentiation ($r_{P/D}$, Eq (8)) is plotted versus initial mesh size, rate of increase in mesh size ($d\xi/dt$), and shear modulus G in Figure 9. The value of $r_{P/D}$ scales with $\xi^{5.7}$ and $G^{-3.2}$, which is in reasonable agreement with the scaling of G with $\xi^{-1/2}$ predicted by Eqs (5) and (6). Since the molecular weight between crosslinks determines both the mesh size and shear modulus, it is difficult to separate the effects of these two parameters on proliferation and differentiation of cells in crosslinked polymers. Previous studies have shown that the elastic modulus of the matrix affects cellular outcomes in both 2D and 3D culture [33, 34]. Naïve MSCs cultured on 2D compliant polyacrylamide hydrogels with moduli comparable to brain tissue (0.1 – 1 kPa) expressed neurogenic markers, while MSCs cultured on rigid matrices approximating osteoid (25 – 40 kPa) expressed osteogenic markers in the absence of differentiation media or growth factors [35]. Other studies have investigated the effects of alginate gel rigidity on cell proliferation on 2D surfaces. Proliferation of rat BMSCs on 2D alginate gels has been reported to decrease as alginate concentration was increased from 3 to 10 wt% (which is outside the range of concentrations investigated in the present study) [52]. However, in another study, 2D proliferation of MC3T3-E1 cells on the surface of sodium alginate gels increased with shear modulus over the range $6 < G < 37$ kPa, and the proliferation rate scaled with $G^{0.4}$ compared to $G^{-3.2}$ for the present study [36]. Considering that this range of *G* values overlaps with that of the present study, the dramatic difference in scaling of the proliferation rate with modulus between 2D and 3Dsuggests that when the cells are confined in a 3D gel, the mesh size may have a predominant role in regulating cell fate relative to the rigidity of the matrix. Previous studies reporting that cell-substrate interactions within 3D gel networks play a key role in regulating cell proliferation and differentiation further support the notion that mesh size controls cell proliferation and differentiation in 3D alginate gels [18–20, 53]

In the present work, we hypothesized that the microstructure and mechanical properties influence the behavior of cells encapsulated in an alginate gel. MC3T3-E1 pre-osteoblast cells were used as a model system to show that the microstructure of the 3D gel regulates proliferation and differentiation of encapsulated cells. While encapsulation in 3D alginate gels is a promising approach for cell therapy, translation of cell transplantation techniques to the clinic is limited by their high immunogenic potential. A promising solution to reducing host immune reaction is to deliver stem cells harvested from the patient. Future studies are needed to determine the applicability of the findings from the present study to other types of cells, such as human mesenchymal stem cells, which are larger than the MC3T3-E1 cells investigated in the present study.

5. Conclusions

In this study, we investigated the effects of the network mesh size and shear modulus of 3D alginate gels on proliferation and osteogenic differentiation of MC3T3-E1 osteoprogenitor cells. Compliant gels with larger mesh size supported cell proliferation, while rigid gels with smaller mesh size enhanced expression of markers of osteoblast differentiation, suggesting that cellular outcomes in 3D alginate beads are regulated by the nanostructure of the networks. This approach may be potentially useful for the design of cell transplantation vehicles that both localize and maintain the viability of the transplanted cells, as well as regulate cell proliferation and differentiation.

Acknowledgments

The authors gratefully acknowledge funding from the Orthopadic Extremity Trauma Research Program (W81XWH-07-1-0211) and the National Institutes of Health (1R01AR056138-01A2).

References

1. Hernandez RM, Orive G, Murua A, Pedraz JL. Microcapsules and microcarriers for in situ cell delivery. Adv Drug Deliv Rev. 2010; 62:711–30. [PubMed: 20153388]
2. Zhang W, Tucker-Kellogg L, Narmada BC, Venkatraman L, Chang S, Lu Y, et al. Cell-delivery therapeutics for liver regeneration. Adv Drug Deliv Rev. 2010; 62:814–26. [PubMed: 20193722]
3. Mandal BB, Kundu SC. Calcium alginate beads embedded in silk fibroin as 3D dual drug releasing scaffolds. Biomaterials. 2009; 30:5170–7. [PubMed: 19552952]
4. Zhou H, Xu HH. The fast release of stem cells from alginate-fibrin microbeads in injectable scaffolds for bone tissue engineering. Biomaterials. 2011; 32:7503–13. [PubMed: 21757229]
5. Wang C, Gong Y, Lin Y, Shen J, Wang DA. A novel gellan gel-based microcarrier for anchorage-dependent cell delivery. Acta Biomater. 2008; 4:1226–34. [PubMed: 18434266]
6. Wagers AJ, Weissman IL. Plasticity of adult stem cells. Cell. 2004; 116:639–48. [PubMed: 15006347]
7. Mooney DJ, Vandenburgh H. Cell delivery mechanisms for tissue repair. Cell Stem Cell. 2008; 2:205–13. [PubMed: 18371446]
8. Hofmann M, Wollert KC, Meyer GP, Menke A, Arseniev L, Hertenstein B, et al. Monitoring of bone marrow cell homing into the infarcted human myocardium. Circulation. 2005; 111:2198–202. [PubMed: 15851598]
9. Evans SM, Mummery C, Doevendans PA. Progenitor cells for cardiac repair. Seminars in cell & developmental biology. 2007; 18:153–60. [PubMed: 17321172]
10. Orive G, De Castro M, Kong HJ, Hernandez RM, Ponce S, Mooney DJ, et al. Bioactive cell-hydrogel microcapsules for cell-based drug delivery. J Control Release. 2009; 135:203–10. [PubMed: 19344677]
11. Wang N, Adams G, Buttery L, Falcone FH, Stolnik S. Alginate encapsulation technology supports embryonic stem cells differentiation into insulin-producing cells. J Biotechnol. 2009; 144:304–12. [PubMed: 19686786]
12. Wikstrom J, Elomaa M, Syvajarvi H, Kuokkanen J, Yliperttula M, Honkakoski P, et al. Alginate-based microencapsulation of retinal pigment epithelial cell line for cell therapy. Biomaterials. 2008; 29:869–76. [PubMed: 18045685]
13. Chen CS, Mrksich M, Huang S, Whitesides GM, Ingber DE. Geometric control of cell life and death. Science. 1997; 276:1425–8. [PubMed: 9162012]
14. Burdick JA, Vunjak-Novakovic G. Engineered microenvironments for controlled stem cell differentiation. Tissue Eng Part A. 2009; 15:205–19. [PubMed: 18694293]
15. Singhvi R, Kumar A, Lopez GP, Stephanopoulos GN, Wang DI, Whitesides GM, et al. Engineering cell shape and function. Science. 1994; 264:696–8. [PubMed: 8171320]
16. Lim JY, Donahue HJ. Cell sensing and response to micro- and nanostructured surfaces produced by chemical and topographic patterning. Tissue Eng. 2007; 13:1879–91. [PubMed: 17583997]
17. Fuhrmann T, Hillen LM, Montzka K, Woltje M, Brook GA. Cell-cell interactions of human neural progenitor-derived astrocytes within a microstructured 3D-scaffold. Biomaterials. 2010; 31:7705–15. [PubMed: 20656342]
18. Kuppers M, Faust D, Linz B, Dietrich C. Regulation of ERK1/2 activity upon contact inhibition in fibroblasts. Biochem Biophys Res Commun. 2011; 406:483–7. [PubMed: 21334310]
19. Eagle H, Levine EM. Growth regulatory effects of cellular interaction. Nature. 1967; 213:1102–6. [PubMed: 6029791]
20. Zeng Q, Hong W. The emerging role of the hippo pathway in cell contact inhibition, organ size control, and cancer development in mammals. Cancer Cell. 2008; 13:188–92. [PubMed: 18328423]
21. Chan AW, Neufeld RJ. Tuneable semi-synthetic network alginate for absorptive encapsulation and controlled release of protein therapeutics. Biomaterials. 2010; 31:9040–7. [PubMed: 20739057]
22. Bouhadir KH, Lee KY, Alsberg E, Damm KL, Anderson KW, Mooney DJ. Degradation of partially oxidized alginate and its potential application for tissue engineering. Biotechnol Prog. 2001; 17:945–50. [PubMed: 11587588]

23. Zhao L, Weir MD, Xu HH. An injectable calcium phosphate-alginate hydrogel-umbilical cord mesenchymal stem cell paste for bone tissue engineering. Biomaterials. 2010; 31:6502–10. [PubMed: 20570346]
24. Jeon O, Bouhadir KH, Mansour JM, Alsberg E. Photocrosslinked alginate hydrogels with tunable biodegradation rates and mechanical properties. Biomaterials. 2009; 30:2724–34. [PubMed: 19201462]
25. Rowley JA, Madlambayan G, Mooney DJ. Alginate hydrogels as synthetic extracellular matrix materials. Biomaterials. 1999; 20:45–53. [PubMed: 9916770]
26. Evangelista MB, Hsiong SX, Fernandes R, Sampaio P, Kong HJ, Barrias CC, et al. Upregulation of bone cell differentiation through immobilization within a synthetic extracellular matrix. Biomaterials. 2007; 28:3644–55. [PubMed: 17532040]
27. Augst AD, Kong HJ, Mooney DJ. Alginate hydrogels as biomaterials. Macromol Biosci. 2006; 6:623–33. [PubMed: 16881042]
28. Rowley JA, Mooney DJ. Alginate type and RGD density control myoblast phenotype. J Biomed Mater Res. 2002; 60:217–23. [PubMed: 11857427]
29. Comisar WA, Kazmers NH, Mooney DJ, Linderman JJ. Engineering RGD nanopatterned hydrogels to control preosteoblast behavior: a combined computational and experimental approach. Biomaterials. 2007; 28:4409–17. [PubMed: 17619056]
30. Fonseca KB, Bidarra SJ, Oliveira MJ, Granja PL, Barrias CC. Molecularly designed alginate hydrogels susceptible to local proteolysis as three-dimensional cellular microenvironments. Acta Biomater. 2011; 7:1674–82. [PubMed: 21193068]
31. Jeon O, Powell C, Ahmed SM, Alsberg E. Biodegradable, photocrosslinked alginate hydrogels with independently tail orable physical properties and cell adhesivity. Tissue Eng Part A. 2010; 16:2915–25. [PubMed: 20486798]
32. Zimmermann U, Thurmer F, Jork A, Weber M, Mimietz S, Hillgartner M, et al. A novel class of amitogenic alginate microcapsules for long-term immunoisolated transplantation. Ann N Y Acad Sci. 2001; 944:199–215. [PubMed: 11797670]
33. Discher DE, Janmey P, Wang YL. Tissue cells feel and respond to the stiffness of their substrate. Science. 2005; 310:1139–43. [PubMed: 16293750]
34. Choi BG, Park MH, Cho SH, Joo MK, Oh HJ, Kim EH, et al. In situ thermal gelling polypeptide for chondrocytes 3D culture. Biomaterials. 2010; 31:9266–72. [PubMed: 20864172]
35. Engler AJ, Sen S, Sweeney HL, Discher DE. Matrix Elasticity Directs Stem Cell Lineage Specification. Cell. 2006; 126:677–89. [PubMed: 16923388]
36. Kong HJ, Liu J, Riddle K, Matsumoto T, Leach K, Mooney DJ. Non-viral gene delivery regulated by stiffness of cell adhesion substrates. Nature materials. 2005; 4:460–4.
37. Taqvi S, Roy K. Influence of scaffold physical properties and stromal cell coculture on hematopoietic differentiation of mouse embryonic stem cells. Biomaterials. 2006; 27:6024–31. [PubMed: 16959314]
38. Gilbert PM, Havenstrite KL, Magnusson KE, Sacco A, Leonardi NA, Kraft P, et al. Substrate elasticity regulates skeletal muscle stem cell self-renewal in culture. Science. 2010; 329:1078–81. [PubMed: 20647425]
39. Ruppender NS, Merkel AR, Martin TJ, Mundy GR, Sterling JA, Guelcher SA. Matrix rigidity induces osteolytic gene expression of metastatic breast cancer cells. PLoS ONE. 2010; 5:e15451. [PubMed: 21085597]
40. Sperling, LH. Introduction to Physical Polymer Science. 3. New York: Wiley-Interscience; 2001.
41. Raeber GP, Lutolf MP, Hubbell JA. Molecularly engineered PEG hydrogels: a novel model system for proteolytically mediated cell migration. Biophys J. 2005; 89:1374–88. [PubMed: 15923238]
42. Smidsrod O. Soution properties of alginate. Carbohydr Res. 1970; 13:359–72.
43. Chan AW, Neufeld RJ. Modeling the controllable pH-responsive swelling and pore size of networked alginate based biomaterials. Biomaterials. 2009; 30:6119–29. [PubMed: 19660810]
44. Caykara T, Inam R. Determination of Average Molecular Weight Between Crosslinks and Polymer–Solvent Interaction Parameters of Poly (acrylamide-g-ethylene diamine tetraacetic acid) Polyelectrolyte Hydrogels. J Appl Polym Sci. 2004; 91:2168–75.

45. Amsden B, Turner N. Diffusion characteristics of calcium alginate gels. Biotechnol Bioeng. 1999; 65:605–10. [PubMed: 10516587]
46. Moe ST, Draget KI, Skjak-Braek G, Smidsrod O. Temperature dependence of the elastic modulus of alginate gels. Carbohydr Polym. 1992; 19:279–84.
47. Jeon O, Song SJ, Lee K-J, Park MH, Lee S-H, Hahn SK, et al. Mechanical properties and degradation behaviors of hyaluronic acid hydrogels cross-linked at various cross-linking densities. Carbohydr Polym. 2007; 70:251–7.
48. Lee KY, Mooney DJ. Alginate: properties and biomedical applications. Prog Polym Sci. 2010
49. Davidovich-Pinhas M, Bianco-Peled H. A quantitative analysis of alginate swelling. Carbohydr Polym. 2010; 79:1020–7.
50. Kong HJ, Lee KY, Mooney DJ. A quantitative analysis of alginate swelling. Macromolecules. 2003; 36:7887–90.
51. Martinsen A, Storro I, Skjark-Braek G. Alginate as immobilization material: III. Diffusional properties Biotechnol Bioeng. 1992; 39:186–94.
52. West ER, Xu M, Woodruff TK, Shea LD. Physical properties of alginate hydrogels and their effects on in vitro follicle development. Biomaterials. 2007; 28:4439–48. [PubMed: 17643486]
53. Abbah SA, Lu WW, Chan D, Cheung KM, Liu WG, Zhao F, et al. Osteogenic behavior of alginate encapsulated bone marrow stromal cells: an in vitro study. J Mater Sci Mater Med. 2008; 19:2113–9. [PubMed: 17136608]

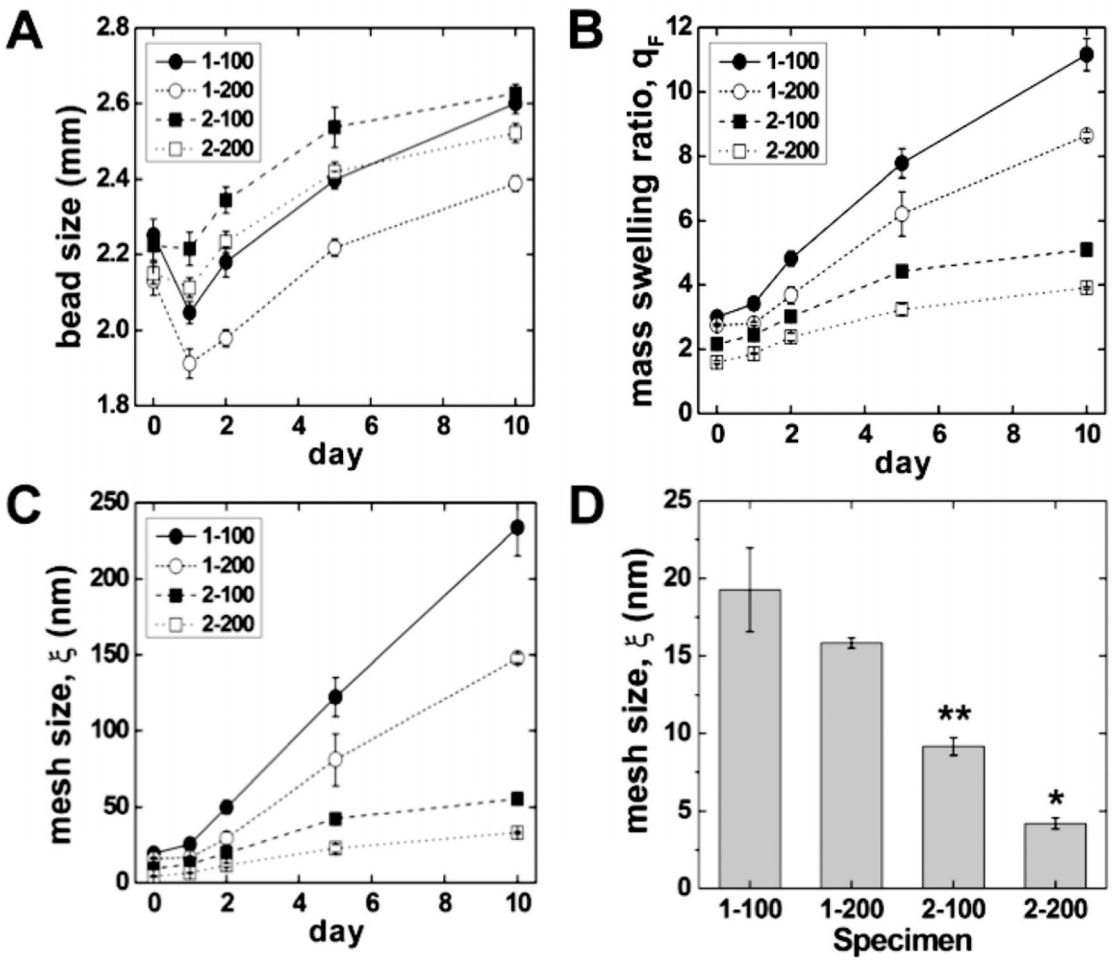

Figure 1.

(A) Size, (B) mass swelling ratio, and (C) calculated mesh size (ξ) of alginate beads measured as a function of immersion time in DI water for up to 10 days. The initial sizes of the 1-100 and 2-100 beads were significantly larger than those of the 1-200 and 2-200 beads ($p < 0.05$). (D) Initial mesh size of synthesized alginate beads. * denotes statistical significance ($p < 0.05$) compared with the 2-200 bead group and all other groups. ** denotes statistical significance ($p < 0.05$) compared with the 2-100 bead group and 1 wt. % groups. The initial mass swelling ratio followed a similar trend as the initial mesh size. By day 2 differences in mesh size and swelling ratio between all groups were significant ($p < 0.05$).

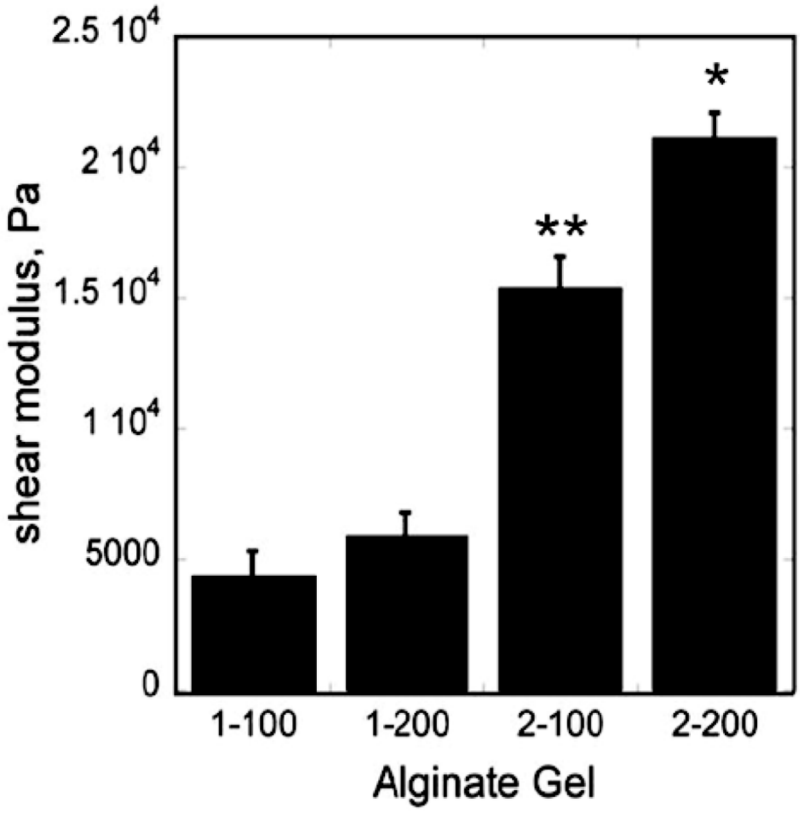

Figure 2.
Elastic moduli of 1-100, 1-200, 2-100, and 2-200 alginate gels measured under shear mode of deformation. Data are presented as average ± standard deviation (n = 3). * denotes statistical significance ($p < 0.05$) compared with the 2-200 bead group and all other groups. ** denotes statistical significance ($p < 0.05$) compared with the 2-100 bead group and 1 wt. % groups.

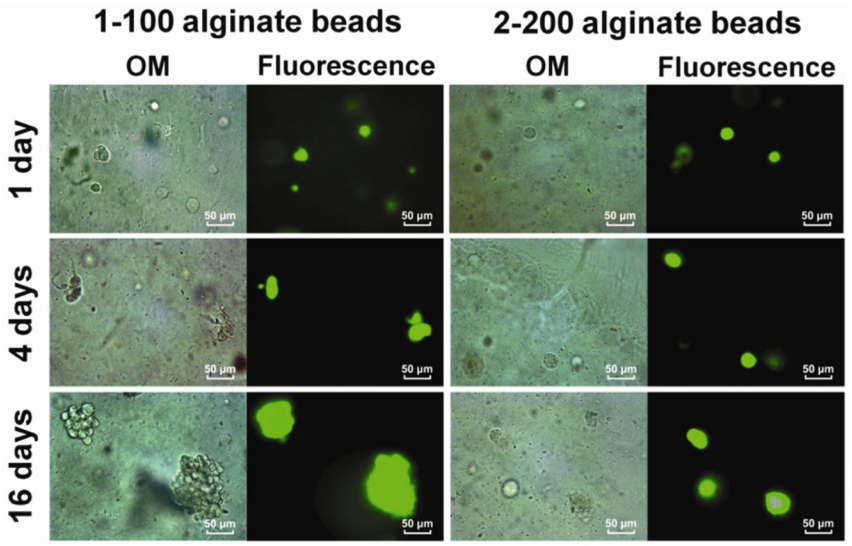

Figure 3.
Optical and fluorescence microscopy images of MC3T3-E1 cells encapsulated in 1-100 and 2-200 alginate beads treated with Live/Dead stain. Beads were cultured in the standard medium for days 1, 4 and 16.

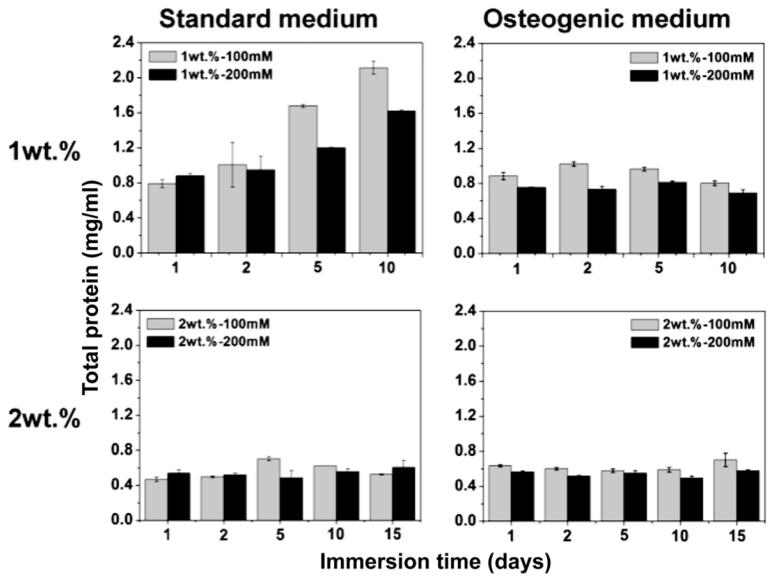

Figure 4.
Total protein (TP) concentration (mg/ml) measured for 5 alginate beads as a function of culture time under dynamic conditions in standard and osteogenic media.

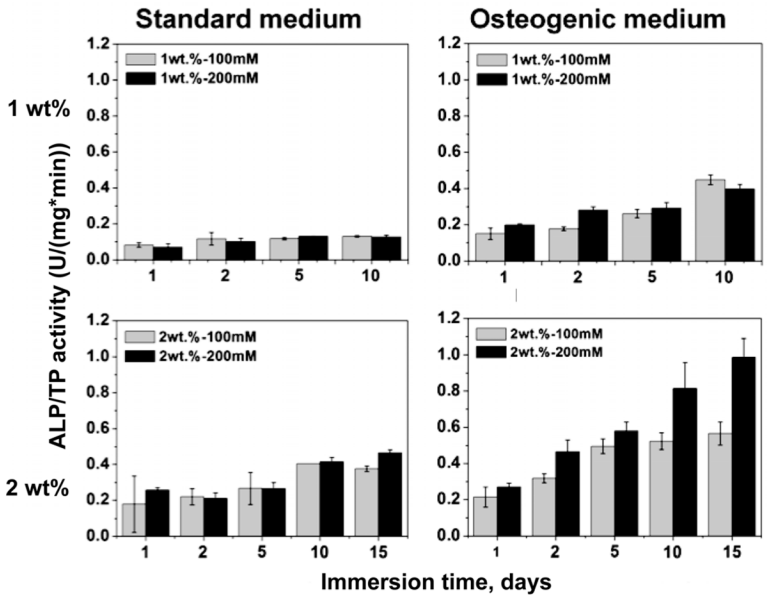

Figure 5.
Alkaline phosphatase (ALP) activity (U/mg/min) measured for 5 alginate beads and normalized by total protein concentration as a function of culture time under dynamic conditions in standard and osteogenic media.

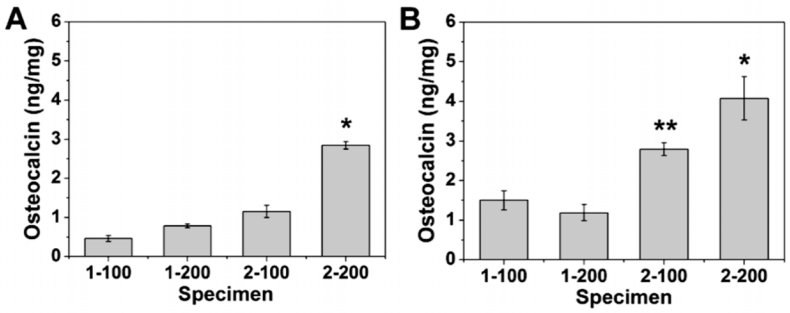

Figure 6.

Osteocalcin secretion by encapsulated MC3T3-E1 cells in alginate beads cultured under dynamic conditions in (A) standard and (B) osteogenic medium for 16 days. (* denotes statistical significance ($p < 0.05$) compared with the 2-200 bead group and all other groups. ** denotes statistical significance ($p < 0.05$) compared with the 2-100 bead group and 1 wt. % groups).

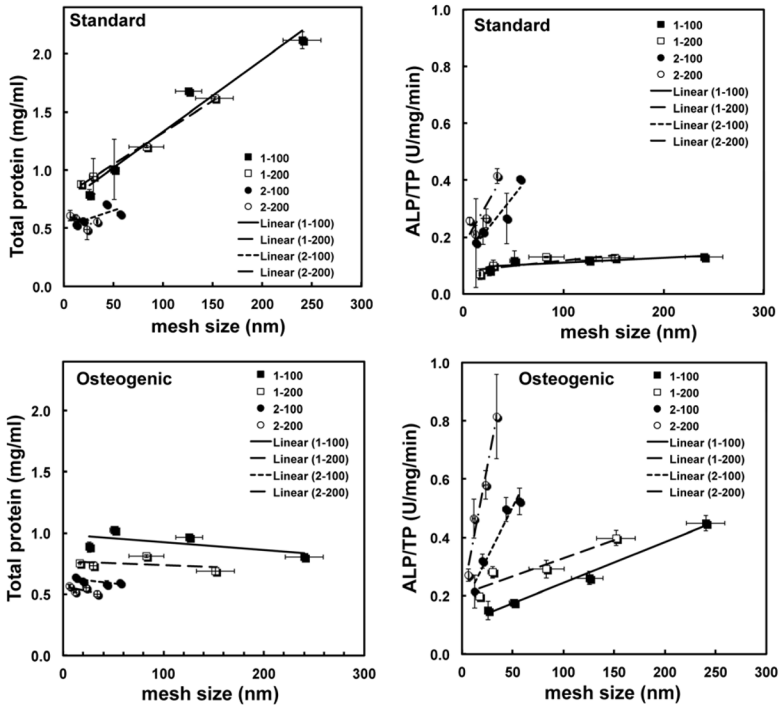

Figure 7.

Total protein (TP) and alkaline phosphatase activity normalized by total protein (ALP/TP) versus alginate mesh size in standard and osteogenic medium for 1-100, 1-200, 2-100, and 2-200 beads. Data were fit to a straight line by linear regression.

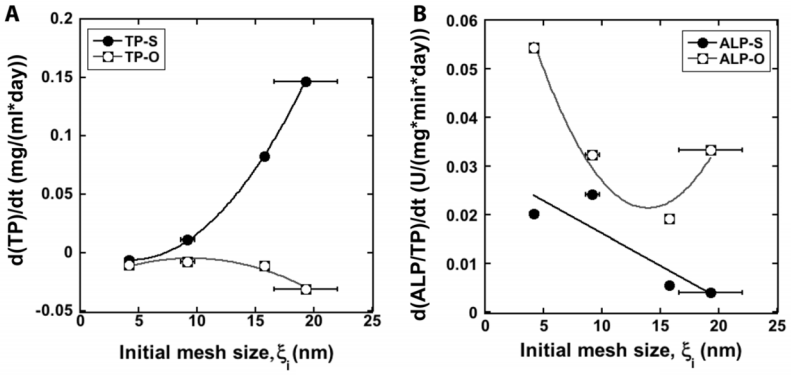

Figure 8.

(A) Proliferation rate (as measured by d(TP)/dt) versus initial mesh size (ξ_i) for standard (TP-S) and osteogenic (TP-O) media. (B) Differentiation rate (as measured by d(ALP/TP)/dt) versus initial mesh size (ξ_i) for standard (TP-S) and osteogenic (TP-O) media.

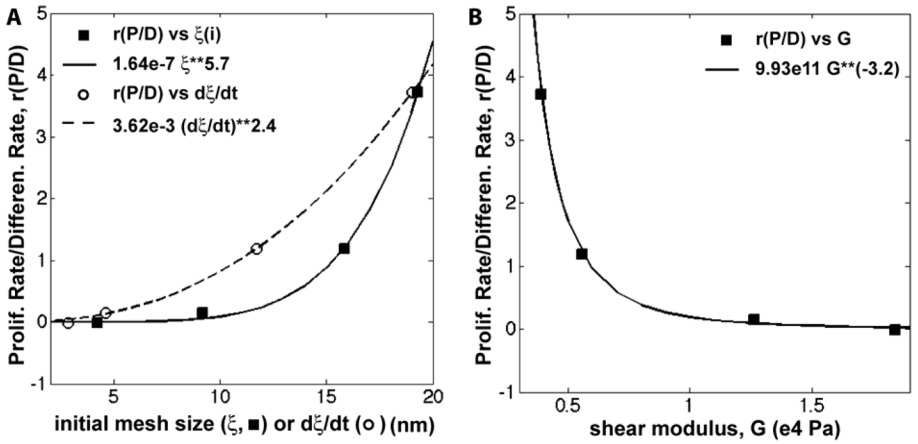

Figure 9.

Ratio of the dimensionless proliferation:differentiation rates ($r_{P/D}$). (A) $r_{P/D}$ versus initial mesh size (ξ_i), represented by filled squares, and versus dξ/dt, represented by open circles. (B) $r_{P/D}$ versus alginate gel shear modulus (G). Data were fit to the power law model (fits shown on the plots).

Table 1

Composition and initial properties of alginate beads.

				Mc, g/mol		Mesh size (ξ), nm	
Bead	**Alginate wt%**	**$CaCl_2$ mM**	**v^2 vol%**	**Swelling**	**Rheology**	**Swelling**	**Rheology**
1–100	1.0	100	0.239 ± 0.018	2674 ± 617	6518 ± 1287	19.3 ± 2.7	30.0 ± 2.7
1–200	1.0	200	0.264 ± 0.003	1921 ± 59	4510 ± 670	15.8 ± 0.3	24.2 ± 1.7
2–100	2.0	100	0.351 ± 0.011	781 ± 85	3942 ± 346	9.2 ± 0.6	14.2 ± 0.8
2–200	2.0	200	0.513 ± 0.021	211 ± 30	2692 ± 6	4.2 ± 0.4	10.6 ± 0.1